Heliyon 10 (2024) e29338

Contents lists available at ScienceDirect

Heliyon

journal homepage: www.cell.com/heliyon

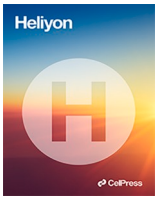

Research article

Multiple inborn errors of type I IFN immunity in a 33-year-old male with a fatal case of COVID-19

Narjes Saheb Sharif-Askari [a,b], Shirin Hafezi [a], Fatemeh Saheb Sharif-Askari [a,c], Hawra Ali Hussain Alsayed [d], Samrein B. M. Ahmed [e], Habiba S. Alsafar [f,g,h], Rabih Halwani [a,b,i,*]

[a] *Research Institute for Medical and Health Sciences, University of Sharjah, Sharjah, United Arab Emirates*
[b] *Department of Clinical Sciences, College of Medicine, University of Sharjah, Sharjah, United Arab Emirates*
[c] *Department of pharmacy practice and pharmacotherapeutics, College of pharmacy, University of Sharjah, Sharjah, United Arab Emirates*
[d] *Department of Pharmacy, Rashid Hospital, Dubai Academic Health Corporation, Dubai, United Arab Emirates*
[e] *Department of Biosciences and Chemistry, College of Health, Wellbeing and Life Sciences, Sheffield Hallam University, Sheffield, S1 1WB, UK*
[f] *Center for Biotechnology, Khalifa University of Science and Technology, Abu Dhabi, United Arab Emirates*
[g] *Department of Biomedical Engineering, College of Engineering, Khalifa University of Science and Technology, Abu Dhabi, United Arab Emirates*
[h] *Department of Genetics and Molecular Biology, College of Medicine and Health Sciences, Khalifa University of Science and Technology, Abu Dhabi, United Arab Emirates*
[i] *Prince Abdullah Ben Khaled Celiac Disease Research Chair, department of pediatrics, Faculty of Medicine, King Saud University, Saudi Arabia*

A B S T R A C T

The host genetic inborn errors of immunity (IEIs) have been shown to contribute to susceptibility to life-threatening coronavirus disease 2019 (COVID-19), as it had been associated previously with other viral infections. Most genetic association studies have described IEIs as a monogenic defect, while there have been no reports of patients with multiple inherited immune deficiencies. This is a complex case of IEIs predisposing to severe viral infections in an unvaccinated 33-year-old male patient. The patient was admitted with no respiratory symptoms, showed a SARS-CoV-2 PCR positive test on the second day of admission, started developing progressive lung consolidation within three days of hospitalization, and was moved from non-invasive to mechanical ventilation within 12 days of hospitalization. Impaired production of type I IFN was detected in patient PBMCs treated with poly(I:C), at both mRNA and protein levels. Whole exome sequencing revealed three mutations across type I IFN production pathway, which were predicted to be loss-of-function (pLOF). The three mutations were predicted to predispose to severe viral infections: monoallelic R488X TLR3, monoallelic His684Arg TLR3, and biallelic Val363Met IRF3. Functional analysis confirmed that all these mutations dysregulated the type I IFN pathway. Evaluation of TLR3 and IRF3 IFN-β1 luciferase reporter activity showed a hypomorphic suppression of function. TOPO TA cloning was used to ascertain the positioning of both TLR3 variants, indicating that both variants were on the same allele. We have described a unique complex IEI patient with multiple mutations, particularly along type I IFN production pathway.

1. Introduction

The presentation of coronavirus disease 2019 (COVID-19), caused by severe acute respiratory syndrome coronavirus 2 (SARS-CoV-2), varied with the host's acquired and genetic risk factors, ranging from asymptomatic infection to life-threatening disease [1–4]. The host genetic inborn errors of immunity (IEIs) have contributed to susceptibility to life-threatening COVID-19, as it had been associated previously with other viral infections, including influenza [5–7] and herpes simplex encephalitis [8,9]. The early genome sequencing

* Corresponding author. College of Medicine, University of Sharjah, Sharjah, United Arab Emirates.
E-mail address: rhalwani@sharjah.ac.ae (R. Halwani).

https://doi.org/10.1016/j.heliyon.2024.e29338
Received 3 November 2023; Received in revised form 4 April 2024; Accepted 5 April 2024
Available online 10 April 2024

studies screened for the severe influenza susceptibility genetic loci within the severe COVID-19 cohort targeting the TLR3 and IRF7 dependent type I IFN pathways [10–12]. While the emerging genome-wide association studies (GWAS) with an untargeted approach have identified coding and non-coding variants along diverse pathways [13–15]. Many variants from the GWAS study remain to be validated experimentally. Most of the genetic association studies had described IEIs as a monogenic defect that underlies the critical viral infections, few had reported cases with two monogenic IEIs [10,16–19], while there have been no reports of patients with multiple inherited immune deficiencies. Herein, we present the detailed clinical, immunological, and genetic characterization of a unique complex IEI patient with acute hepatitis and critical COVID-19 pneumonia, who had multiple mutations particularly along type I IFN production pathway.

2. Material and methods

2.1. Patients

This study was approved by the Dubai Scientific Research Ethics Committee (DSREC-04/2020_19). Written, informed consent was obtained from all study participants prior to inclusion and included publishing the genetic results and x-ray scan. Participants for the study were recruited from Rashid Hospital in Dubai, UAE. Non-infected individuals and those diagnosed with COVID-19 were included. Diagnosis of COVID-19 was confirmed through a positive SARS-CoV-2 infection polymerase chain reaction (PCR) test, while non-infected controls were identified through a negative SARS-CoV-2 test. The severity of the COVID-19 patients was evaluated using the National Institutes of Health (NIH) COVID-19 guidelines [20]. Asymptomatic cases were defined as those who did not present any symptoms at the time of SARS-CoV-2 testing or diagnosis, while severe cases were defined as diseases requiring hospitalization and respiratory support [21–23]. Blood samples were collected from each participant and all necessary precautions, as recommended by the CDC, were taken to ensure safe collection, handling, and testing of biological fluids [24].

2.2. Whole-exome sequencing

The genomic DNA was extracted from whole blood samples using the QIAamp DNA Mini Kit from Qiagen (Valencia CA, USA; catalogue no. 51304). The samples were then sequenced using the Illumina Hiseq 2500 platform and aligned with the human reference genome (hg19) through the maximum exact matches algorithm in Burrows-Wheeler Aligner software [25]. The BAM file was sorted, and PCR duplicates were removed. The Genome Analysis Toolkit (GATK4)'s best practices were utilized to perform variant calling and generate a multi-sample variant call file (VCF) [26]. SnpEff and Annovar software were utilized to annotate and predict the functional effects of variants on genes, following the receipt of a multi-sample VCF file. Variants with a minor allele frequency (MAF) of less than 1 % in the ExAc database were selected. Additionally, the viral and influenza susceptibility genes that underwent study through the COVID Human Genetics Effort (CHGE, www.covidhge.com) were taken into consideration [10,16,27,28].

2.3. Sanger sequencing

The coding sequence of TLR3 and IRF3 variants was amplified from genomic DNA using specially designed primers. The variant was then validated in both the forward and reverse directions using Sanger sequencing to exclude any NGS artifacts. A sequencing primer was designed to amplify the respective exon and the flanking two introns. Genomic DNA was extracted from whole blood samples using the QIAamp DNA Mini Kit (catalog no. 51304) from Qiagen, Valencia CA, USA. Sequencing was carried out in both directions using the ABI BigDye Terminator v.3.0 kit. The products were resolved using capillary electrophoresis on an ABI 3500 capillary sequencer (ABI 3500 Genetic Analyzer, Applied Biosystems).

2.4. Computational Analysis of the mutants

Protein modeling was performed using the Pymol program (pymol.org). Human TLR3 extracellular domain (ectodomain) structure (PDB accession number 1ZIW) [29] was used to illustrate c.1462C > T (p. Arg488*) and c. 2051A > G (p. His684Arg) variants, while the phosphorylated TRIF in complex with IRF3 structure (PDB accession number 5JEL) [30] was used to illustrate c.982C > T (p. Val363Met) variant. The degree of evolutionary conservation of amino acids was estimated using ConSurf [31]. The amino acid conservation was scored between 1 and 9 to reflect low and high conservation degrees, respectively. Additionally, following the neural-network algorithm, each amino acid was predicted as buried (b) or exposed (e) and assessed as functional (f) or structural (s) residue [31]. Furthermore, in silico protein prediction algorithms (SIFT, PolyPhen, CADD) were used to predict the effect of the selected mutation.

2.5. qRT-PCR

The isolated PBMCs from the severe COVID-19 case and the 5 asymptomatic patients were treated with 1 μg/ml of Human IFN-α2a (Miltenyi Biotec, Bergisch Gladbach, Germany; catalog no. 130-093-874) or 25 μg/ml of poly(I:C) (Sigma-Aldrich, MO, USA; catalog no. P1530) for the duration of 24 h. Total RNA from PBMCs was isolated using Trizol reagent according to the manufacturer's instructions (Invitrogen, CA, USA; catalog no. 15596-018) [32]. Complementary cDNA was synthesized from 1 μg of RNA using the High-Capacity cDNA Reverse Transcription Kit (Applied Biosystems, CA, USA; catalog no. 4368814) according to the manufacturer's

protocol. For cDNA amplification, 5x Hot FirePol EvaGreen qRT-PCR SuperMix (Solis Biodyne, Tartu, Estonia; catalog no. 08-36-00008) was used, and qRT-PCR was performed in QuantStudio 3 Real-Time PCR System (Applied Biosystems, CA, USA) [33]. The following primers were used: IFNA1 forward CCAGCAGATCTTCAACCTCTTT and reverse CAAGTCATTCAGCTGCTGGTAG; IFNB1 forward CCTGTGGCAATTGAATGGGAGGC and reverse AGATGGTCAATGCGGCGTCCTC; ISG-15 forward TGGGACCTGACGGTGAAGATGC and reverse GCACGCCGATCTTCTGGGTGAT; IFTIM3 forward CATGTCGTCTGGTCCCTGTTC and reverse ATCCATAGGCCTGGAAGATCAGC; and 18s forward TGACTCAACACGGGAAACC and reverse TCGCTCCACCAACTAAGAAC. Gene expression was analyzed using the Comparative Ct (ΔΔCt) method upon normalization to the reference gene 18s rRNA [34]. Unpaired student t-test was used to compare the independent groups. (GraphPad Software, San Diego, Calif). For all analyses, P-values <0.05 were considered significant.

2.6. Western blot

The peripheral blood mononuclear cell (PBMCs) from the severe COVID-19 case and the 5 asymptomatic patients were isolated from whole blood using standard Ficoll-Paque density gradient centrifugation (Histopaque, Sigma-Aldrich, MO, USA; catalog no. 10771). The isolated PBMCs were treated with 25 μg/ml of poly(I:C) (Sigma-Aldrich, MO, USA; catalog no. P1530) for duration of 24 h. PBMCs were homogenized in lysis buffer containing RIPA lysis buffer 1X and a cocktail of inhibitors (1 mM PMSF and a protease inhibitor cocktail (Sigma-Aldrich, Germany; catalog no. P2714). After lysis, the concentration of proteins was determined using the Thermo Scientific Pierce BCA Protein Assay Kit. The cell lysates were diluted in 1X Laemelli's buffer solution at 95 °C for 5 min. Total protein (10 μg/lane) was separated on 12 % SDS-polyacrylamide gels and then transferred onto nitrocellulose membranes (Amersham, Germany) by the semi-dry transfer system (Bio-Rad, Ca, USA). The membranes were blocked with 5 % BSA in Tween Tris-Buffered saline (TTBS) for 1h and incubated with primary TLR3 (Abcam, 1:1000; catalog no. ab62566) or RIG1 (Cell Signaling, 1:1000; catalog no. 3743) or MX1 (Cell Signaling, 1:1000; catalog no. 37849) or β-actin (Cell Signaling, 1:1000; catalog no. 8457) antibodies at 4 °C overnight and then with secondary anti-rabbit IgG (catalog no. 7074, 1:1000) antibody conjugated to horseradish peroxidase for 1 h at room temperature. The blots were visualized with enhanced chemiluminescence (ECL) kit (using the ECL™ Prime Western Blotting System GE Healthcare, RPN2232) and imaged using ChemiDoc™ Touch Imaging System (Bio-Rad, Ca, USA).

2.7. IFN-β elisa assay

The isolated PBMCs were cultured in 6-well microtiter plates (1×10^6 cells/well in 2 mL RPMI 1640 media; Sigma, Poole, United Kingdom) at 37 °C with 5 % CO_2. The cells were treated with 25 μg/ml of poly(I:C) (Sigma-Aldrich, MO, USA; catalog no. P1530) for a duration of 24 h. The level of IFN-β protein production was determined in the culture supernatant using a commercially available human ELISA kit (IFN-β, Abcam, Cambridge, MA, USA; catalog no. ab278127). Assays were performed strictly following the manufacturer's instructions. Each sample was assayed in duplicate, and values were expressed as the mean of 2 measures per sample. One-way analysis of variance (ANOVA) and post hoc Tukey multiple comparison analyses were applied.

2.8. Anti-IFN autoantibodies ELISA assay

Plasma samples from the severe COVID-19 case and the 5 asymptomatic cases were isolated from blood via standard centrifugation. Elisa was performed as described previously [35]. Briefly, 96-well ELISA plates (Nunc-Immuno™ MicroWell™ 96 well solid plates; Thermo Fisher Scientific, MA, USA; catalog no. 167008) were coated by incubation overnight at 4 °C with human IFN-α2 recombinant protein (2 μg/ml; Miltenyi Biotec, Bergisch Gladbach, Germany; catalog no. 130-093-874) and human IFN-ω recombinant protein (eBioscience, CA, USA; catalog no. BMS304). Coated plates were then washed (PBS, 0.005 % Tween 20), blocked by incubation with 5 % nonfat milk powder in the same buffer, washed, and incubated with 1:250 dilutions of plasma from the patients or controls for 2 h at room temperature. Horseradish peroxidase (HRP)-labelled anti-human IgG, IgM or IgA (Abcam, Cambridge, MA, USA; catalog no. ab102420) was added to a final concentration of 2 μg/ml. To develop the plate, 100 μl/well of TMB substrate solution (TMB Substrate Kit, Thermo Fisher Scientific, MA, USA; catalog no. 34021) was added and incubated for 5 min. The reaction was stopped with 2 M sulfuric acid (100 μl/well) and optical density at 450/630 nm was measured via BioTek EL808 microplate reader.

2.9. IFN-β1 luciferase reporter assay

HEK293T cells were cotransfected with IFN-β1 firefly luciferase reporter construct, renilla luciferase plasmid, and TLR3 or IRF3 constructs using ViaFect transfection reagent (Promega, Madison, USA; catalog no. E4982). The pcDNA3-TLR3-CFP plasmid was a gift from Dr. Douglas Golenbock (Addgene; catalog no. 13641), the V5-IRF3-pcDNA3 was a gift from Saumen Sarkar (Addgene; catalog no. 32713) [36], while the IFN-β1 firefly and pRL-TK-Renilla luciferase plasmids were a gift from Jean-Laurent Casanova. The TLR3 and IRF3 variants of the patient in our analysis were generated by site-directed mutagenesis (QuikChange II XL site-directed kit; Agilent Technologies, USA; catalogue no. 200522) and later confirmed by Sanger sequencing. For transfection HEK293T cells were seeded in 6-well plates and cultured in complete media (DMEM, 10 % fetal bovine serum and 1 % Pen-Strep; Sigma-Aldrich, MO, USA). Briefly, for one well of 6-well plate, 0.75 μg of IFN-β1 firefly luciferase reporter construct and 1 μg of either *TLR3* or *IRF3* constructs were mixed in 200 μL of DMEM media. The vector solution was then mixed with 6 μL of ViaFect solution and subsequently incubated at room temperature for 10 min. The respective transfection mix (200 μl/well) was then applied in a dropwise manner to each well already supplemented with 1.8 ml of fresh media. The plates were then returned to 37 °C in a humidified atmosphere with 5 % CO_2 for 24 h.

The transfected cells were treated after 24 h with 25 μg/ml poly(I:C) (Sigma-Aldrich, MO, USA; catalog no. P1530) for 6 h. The luciferase assay was carried out by using the Dual Luciferase Assay System (Promega, Madison, Wis, USA; catalog no. E1910) according to the manufacturer's protocol. Luminescence intensity was measured with a Promega GloMax Discover microplate reader (Promega, Madison, Wis, USA). Firefly luciferase activity values were normalized against Renilla luciferase activity values. The percentage of

Table 1
Basic and clinical characteristics of the proband at admission.

Variables	Values	Reference Range
BP	131/73	
HR	118	
RR	18	
Temperature	37.7	
SPO2 (%)	100	
CBC		
WBC	**28.5 H**	4.1–11.0 $10^3/\mu$
RBC	5.27	4.6–6.10
Hemoglobin	16.3	13.5–18 g/dL
Hematocrit %	51.5	41–53
MCV	**97.7 H**	80–95
MCH	31	27–32
Platelets $10^3/\mu L$	**135 L**	150–450
Neutrophils %	**81.5 H**	35–75
Lymphocyte %	8.7	16.5–52
Monocyte %	**9.3 H**	0–8.0
Eosinophil %	0.1	0–5.0
Basophil %	0.4	0–4.0
Neutrophil Absolute	**23.2 H**	1.8–7.7
Lymphocytes Absolute	2.5	1.2–4.8
Monocytes Absolute	**2.7 H**	0–0.8
Eosinophils Absolute	0	0–0.5
Basophils Absolute	0.1	0–0.2
Liver function test		
Bilirubin, Total	**1.7 H**	0.1–1.2 mg/dL
Alkaline Phosphatase	**294 HH**	44–147 IU/L
AST	**11857 H**	8–45 U/L
ALT	**5335 HH**	7–56 U/L
Albumin	4.2	3.4–5.4 g/dL
Globulin	**3.6 H**	2–3.5 g/dL
Gamma GT (GGT)	**75 H**	0–72 U/L
PT PTT		
Prothrombin Time	**20.9 H**	10–13 s
INR	**1.73 H**	0.8–1.2
APTT	**38.4 H**	22–35 s
Urea Electrolytes		
Sodium	**131 L**	136–145 mmol/L
Potassium	**8 H**	3.5–5 mmol/L
Chloride	**93 L**	98–106 mmol/L
Bicarbonate (HCO3)	**7.3 L**	23–28 mmol/L
Urea	**59 H**	6–24 mg/dL
Anion Gap	**31 H**	4–12 mmol/L
eGFR (CKD-EPI)	**20 L**	60 or more ml/min/1.73 m^2
Creatinine	**3.7 HH**	0.7–1.30 mg/dL
Magnesium blood	2.38	1.6–2.6 mEq/L
Calcium blood	**7.6 L**	8.6–10.6 mg/dL
Phosphate blood	**7.6 H**	2.8–4.5 mg/dL
Lipase	31	12–53 U/L
Glucose	**165 H**	Less than 140 mg/dL
Lactic acid	**17 H**	4.5–19.8 mg/dL
Procalcitonin (PCT)	**17.10 H**	Less than 0.1 ng/ml
C-reactive protein	**14.2 H**	1.0–3.0 mg/L
Ferritin	**51380 H**	10–204 ng/mL
LDH	**6919 H**	105–333 IU/L
CK total	**1156 H**	24–204 U/L
BNP	**11,123 H**	Less than 100 pg/ml

ALT: Alanine aminotransferase; APTT: activated partial thromboplastin time; AST: aspartate aminotransferase; BNP: B-type natriuretic peptide; BP: blood pressure; CBC: complete blood count; CK: creatine kinase; CKD-EPI: CKD Epidemiology Collaboration (CKD-EPI); eGFR: estimated glomerular filtration rate; H: High; HR: heart rate; INR: international normalized ratio; LDH: Lactate Dehydrogenase; MCH: mean corpuscular hemoglobin; MCV: mean corpuscular volume; PT: prothrombin time; PTT: partial thromboplastin time; RBC: red blood cells; RR: Respiratory rate; SPO2: Oxygen saturation; WBC: white blood cells.

IFN-β1 promoter activity was calculated compared to the WT. One-way analysis of variance (ANOVA) and post hoc Tukey multiple comparison analyses were applied. (GraphPad Software, San Diego, Calif). For all analyses, *P*-values <0.05 were considered significant.

2.10. TOPO TA cloning

The TOPO TA Cloning Kit for sequencing (Carlsbad, CA 92008 USA) was used to clone a PCR product from the proband, following the manufacturer's instructions. The following primers were used: TLR3 forward GCCTTAATGAAATTGGGCAAG and reverse CGATGTACTGAAACATTCCA. The cloning process utilized competent bacteria cells of the Escherichia coli DH5α strain obtained from the Department of Microbiology and Immunology at the Sharjah Institute for Medical Research. The TOPO TA Cloning kit protocol was followed, and the clone was successfully created. Clones were grown overnight on LB agar with kanamycin sulfate (HiMedia, CMS210-5G) for selection (50 μg/ml), after the cloning step. Kanamycin-resistant colonies were picked, and colony PCR was performed. The clones were cultured in Luria-Bertani broth (HiMedia LB broth M575-500G). The final step involved the purification of plasmid by QIA prep Spin Miniprep Kit (Qiagen, Germany). The final product underwent screening through Sanger sequencing.

3. Results

3.1. Case presentation

A 33-year-old male with history of recurrent viral infection, was presented to the hospital with fever, nausea, vomiting, and diarrhea. On admission, blood analysis revealed septic level of procalcitonin (PCT) = 17.10 ng/ml, elevated C-reactive protein (CRP) = 14.2 mg/L and raised white blood count (WBC) = 28.5 10^3/μL. Coagulopathy with an INR of 1.73 and APTT of 38.4 s was documented. The patient was presented with liver and renal injury, having elevated B-type natriuretic peptide (BNP) and creatine kinase (CK) levels of 11123 pg/ml and 1156 U/L, respectively. He was oligouric with a serum creatinine of 3.7 mg/dL and an estimated glomerular filtration rate (eGFR; CKD-EPI) of 20 ml/min/1.73 m^2. Total bilirubin = 1.7 mg/dL, Alkaline Phosphatase (ALP) = 294 IU/L, alanine aminotransferase (ALT) = 5335 U/L, aspartate aminotransferase (AST) = 11857 U/L and gamma glutamyltransferase (GGT) = 75 U/L. The baseline characteristics of the proband are presented in Table 1.

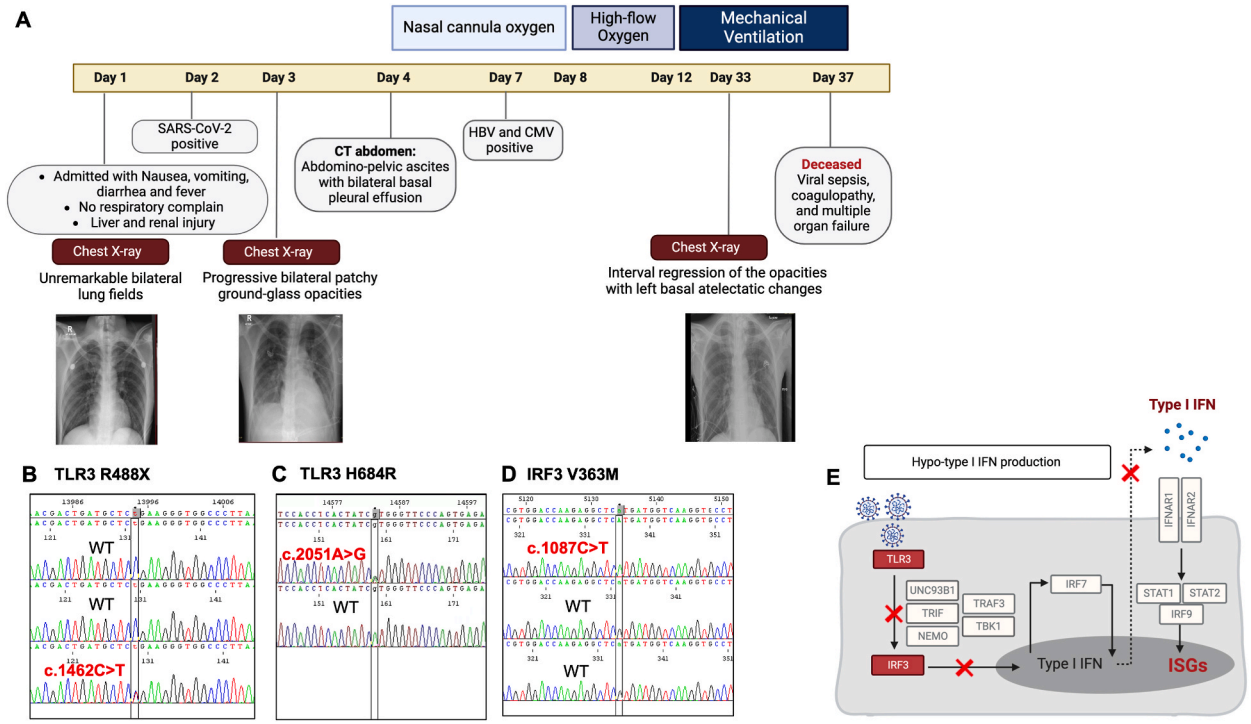

Fig. 1. Multiple inborn errors of type I IFN immunity in a 33-year-old male. **(A)** Patient hospital course timeline (Created with BioRender.com). Chest X-rays were taken on day one, day three, and four days before passing away (day 33). Heterozygous variants c.1462C > T **(B)** and c.2051A > G **(C)** in TLR3, and homozygous variant c.1087C > T **(D)** in IRF3 were identified in the proband. The mutations were confirmed in genomic DNA and cDNA from whole blood samples. The sequence of the polymerase chain reaction products of genomic DNA is shown. **(E)** Type I IFN production and response pathways. The affected genes (TLR3 and IRF3) are marked in red. (For interpretation of the references to colour in this figure legend, the reader is referred to the Web version of this article.)

The Hepatitis B virus (HBV) serological profile was positive for HBsAg and Anti-HBe, while the tests for IgM HBc, HBeAg were negative. RT-PCR tests were positive for Hepatitis B, cytomegalovirus (CMV) and SARS-CoV-2 viruses. He was tested negative for Hepatitis A and C viruses, malaria parasite, and HIV-1/HIV-2 virus. Abdominal CT showed significant increase in the abdomino-pelvic ascites with bilateral basal pleural effusion. Although on admission chest x-ray showed unremarkable bilateral lung fields, the x-ray on third hospitalization day revealed a progressive course regarding bilateral patchy ground-glass opacities. His last chest x-ray (day 33) showed interval regression of the opacities in the right lower zone and the lung fields with left basal atelectatic changes observed (Fig. 1A). The clinical scenario was interpreted as sepsis with coagulopathy, acute hepatitis viral infection, progressive organ failure, and CMV and SARS-CoV-2 viral infections. The patient's disease progressed rapidly; he was moved from non-invasive to mechanical ventilation after 12 days of hospital admission. The patient died from viral sepsis and multiple organ failure after 25 days of receiving intubation.

3.2. Whole-exome and sanger sequencing

Patients' blood was collected, and whole exome sequencing (WES) was conducted, which revealed three mutations within the type I interferon production pathway (Fig. 1B–E). WES data was subjected to GATK4 variant callings pipeline, and the identified variants were filtered according to their Minor allele frequency (MAF). Variants with MAF of less than 1 % were selected and moved to targeted analyses. Based on protein prediction of function tools and protein structural modeling, three variants were selected from the pathway. Sanger sequencing was then performed, which confirmed the presence of two TLR3 variants: NM_003265.3(TLR3):c.1462C > T (p.Arg488*) and NM_003265.3(TLR3):c.2051A > G (p.His684Arg), as well as one IRF3 variant: NM_001571.6(IRF3):c.1087G > T (p.Val363Met) (Fig. 1B–D and Table 2).

3.3. Computational Analysis of the mutants

The study investigated TLR3 and IRF3 variants that were predicted to be associated with a predisposition to respiratory viral infection and hepatitis B**.** The heterozygous TLR3 Arg488* variant (rs772992927) created a stop codon in the middle of TLR3 ecto-domain; it was located within the exon four that also included other COVID-19 associated TLR3 variants, as shown in Fig. 2A–B. The affected protein was predicted to be highly conserved (score 8) exposed residue and of functional significance (Fig. 2C). The second TLR3 variant was a heterozygous TLR3 His684Arg variant (rs1254995294). This sequence change replaced histidine, which is basic and polar, with arginine, which is basic and polar. The histidine at the mutation position was predicted to be a highly conserved amino acid (Score 8; Fig. 2D). The variant was predicted to be probably damaging in PolyPhen-2 but benign in SIFT.

The other variant downstream of TLR3 was a homozygous IRF3 Val363Met variant (rs148672096) located in exon 7 (Fig. 2E). The Valine at the mutation position was predicted to be a buried residue with moderate-high conservation (score 6) (Fig. 2F–G). Furthermore, this variant was presumed to be deleterious based on in silico protein prediction tools, including SIFT and PolyPhen-2.

3.4. Functional analysis of the detected mutants

To confirm Sanger's results, validation experiments were performed for TLR3 and IRF3 variants upstream of the IFN sensing pathway. mRNA and protein levels of the affected genes were determined following poly(I:C) stimulation of PBMCs isolated from the proband and 5 other asymptomatic COVID-19 patients (Table S1).

The results of qRT-PCR analysis showed a significant deficiency in IFN production signaling. Upon stimulation with poly(I:C), there was no increase in the expression levels of IFNα and IFNβ as shown in Fig. 3A. In contrast, patients who were asymptomatic and had no defect in the interferon signaling pathway, showed a considerable increase in both IFNα and IFNβ levels, along with ISG expression levels (Fig. 3A–B).

The Western blot results indicated that the proband exhibited no baseline expression of TLR3, RIG1, and MX1 (Fig. 3C and Fig. S1). Upon poly(I:C) stimulation, TLR3 manifested as a truncated protein, RIG1 displayed a faint band, and MX1 showed no observable band (Fig. 3D and Fig. S2). In contrast, the asymptomatic group exhibited baseline expression of TLR3, RIG1, and MX1, with their expression levels increasing following stimulation (Fig. 3C–D).

The IFNβ production was then determined by running ELISA on PBMCs culture supernatant following 24 h of stimulation with poly (I:C). No change was observed in IFNβ levels in the proband, while the IFNβ levels were significantly increased following stimulation in asymptomatic COVID-19 cases (mean 24.9 ± 8 vs mean 1.5 ± 0.4 pg/ml; p-value <0.0001) (Fig. 3E). We next screened the proband

Table 2
Variants in known IEI genes in the proband.

Chr	Position	Zyg	Consequence	Ref	Alt	Gene	mRNA change	Amino acid change	MAF	CADD score
4	187004302	het	stopgain	C	T	TLR3	c.1462C > T	p. Arg488*	0.0000163	36
4	187004891	het	missense	A	G	TLR3	c. 2051A > G	p.H684R	0.00001	4.89
19	50163981	hom	missense	C	T	IRF3	c.982C > T	p. Val363Met	0.0013	23.5

Alt: alteration variant; CADD: Combined Annotation Dependent Depletion score; Het: heterozygous; Hom: homozygous; MAF: minor allele frequency in gnomAD database (https://gnomad.broadinstitute.org/); Ref: reference allele; Zyg: zygosity.

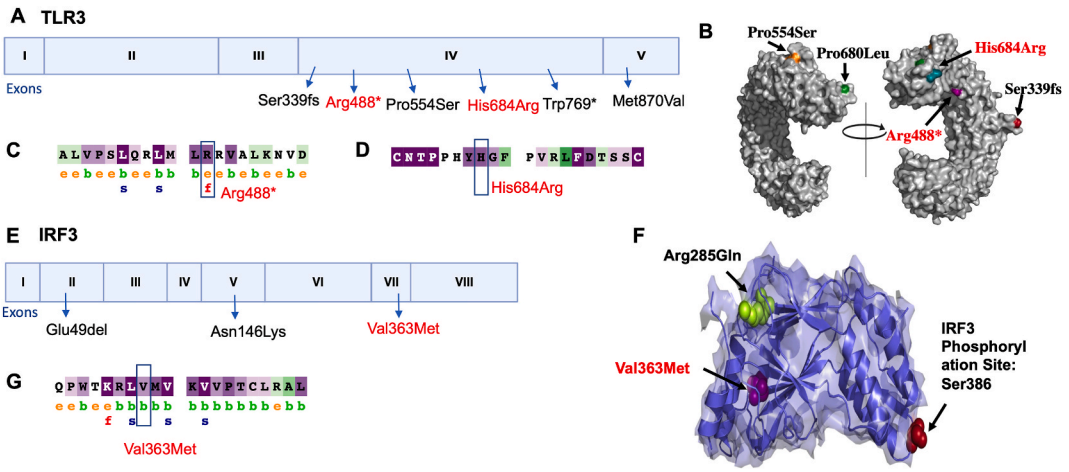

Fig. 2. Computational Analysis of the Mutant. **(A)** Graphical view of the TLR3 variants within exon 4 and 5. The TLR3 Arg488* and His684Arg from the proband are shown in red, and the variants reported by Zhang et al. are marked in black. **(B)** Two views of the human TLR3 ectodomain (ECD). Pro680Leu (shown in orange) was associated with IAV, Pro554Ser (shown in green) was associated with both IAV and COVID-19, while Ser339fs (shown in red) and patient's variant Arg488* (shown in magenta) and His684Arg (shown in green) were associated with COVID-19. The amino acid conservation degree and functional effect of Arg488* **(C)** and His684Arg **(D)** variants were predicted using ConSurf tool. **(E)** A graphical view of the IRF3 variants in GRCh37 assembly. The IRF3 Val363Met variant from the proband is shown in red, and the variants reported by Zhang et al. are marked in black. **(F)** Phosphorylated TRIF in complex with IRF3 structure 3D model. The proband's IRF3 variants **(**Val363Met shown in magenta) nearby the IRF3 phosphorylation site of Ser386 (marked in red). The variant Arg285Gln (shown in limon) was previously associated with impaired IFN responses to HSV-1 infection. **(G)** The amino acid conservation degree and functional effect of the Val363Met variant were predicted using ConSurf tool. (For interpretation of the references to colour in this figure legend, the reader is referred to the Web version of this article.)

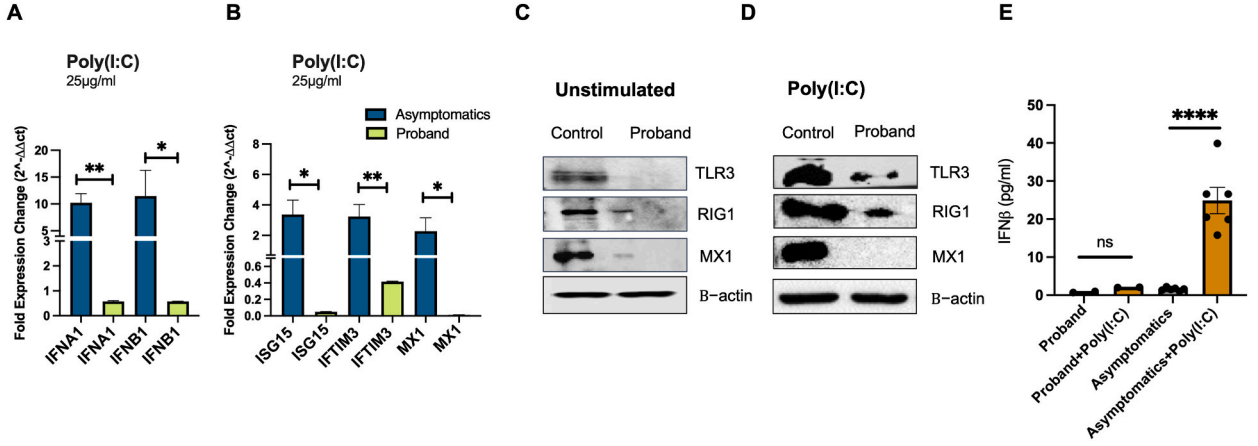

Fig. 3. Impact of type I IFN variants on expression and function. Impaired type I IFN response to poly(I:C) treatments in patient's peripheral blood mononuclear cells (PBMCs). The mRNA levels of **(A)** IFNA1 and IFNB1 and **(B)** interferon-stimulated genes (ISGs) genes following 25 µg/ml of poly (I:C) stimulation for 4 h. Gene expression was analyzed using the Comparative Ct (ΔΔCt) method upon normalization to the reference gene 18s rRNA. Unpaired student t-test was used to compare the independent groups. TLR3, RIG1, and MX1 at **(C)** baseline and **(D)** in poly(I:C) stimulated PBMCs were measured by western blotting. The uncropped full blots of (C) and (D) are deposited in Supplementary Figs. S1 and S2, respectively. **(E)** IFN-β production was measured by ELISA, 24 h after stimulation or not with 25 µg/ml of poly(I:C), in PBMCs from the proband and 5 asymptomatic COVID-19 patients. One-way analysis of variance (ANOVA) and post hoc Tukey multiple comparison analyses were applied.

and asymptomatic COVID-19 patients for serum autoantibodies against IFN-α2 and IFN-ω, and both tested autoantibodies were negative in all patients. Furthermore, the two variants of TLR3 and IRF3 were next evaluated using IFN-β1 luciferase reporter assay. All variants resulted in hypomorphic suppression of function. The relative WT IFN-β1 promoter activity produced by Arg488* TLR3 was 42 %, His684Arg TLR3 was 31 %, and Val363Met IRF3 was 32 %. The results of luciferase reporter assays for TLR3 and IRF3 are presented in Fig. 4A and B, respectively. Due to our inability to obtain blood samples from the parents, we opted for TOPO TA cloning to ascertain the positioning of both TLR3 variants - whether on the same allele or different alleles (cis or trans). The cloning results indicated that both variants were on the same allele (Fig. 4C).

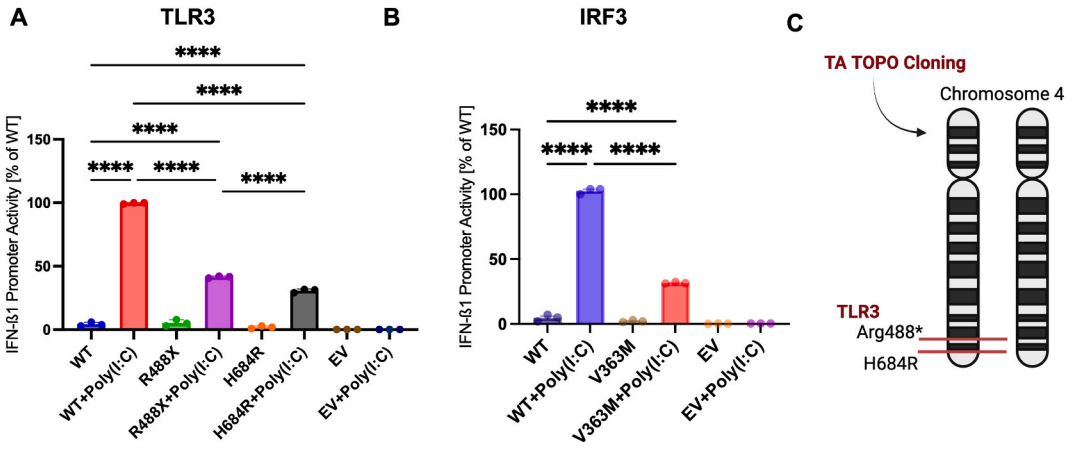

Fig. 4. Site-Directed Mutagenesis and Luciferase Analysis of TLR3 and IRF3 Mutations. **(A and B)** HEK293T cells were transiently transfected with IFNB1 firefly luciferase reporter, Renilla luciferase reporter, and plasmids encoding WT or Mutated (Arg488* TLR3, His684Arg TLR3, or Val363Met IRF3 as indicated). Cells were stimulated or not with 25 μg/ml poly(I:C), and luciferase activities were measured 6 h later. Firefly luciferase activity was normalized to Renilla luciferase activity and presented as percentage stimulation in cells expressing Arg488* TLR3, His684Arg TLR3, or Val363Met IRF3 relative to cells expressing WT TLR3 or IRF3. Data from 3 independent experiments are shown. One-way analysis of variance (ANOVA) and post hoc Tukey multiple comparison analyses were applied. For all analyses, P-values <0.05 were considered significant. **(C)** TOPO-TA cloning was performed to determine the positioning of the TLR3 variants, whether they were located on the same allele or different alleles (cis or trans). The cloning results indicated that both variants were on the same allele (Created with BioRender.com).

4. Discussion

In this case report, we describe an adult patient with several inborn errors of anti-viral IFN immunity that predisposed him to viral infections, including hepatitis B, SARS-CoV-2, and CMV. The patient did not receive any COVID-19 vaccines. The patient was admitted with no respiratory symptoms, showed a SARS-CoV-2 PCR positive test on the second day of admission, started developing progressive lung consolidation within three days of hospitalization, and was moved from non-invasive to mechanical ventilation within 12 days of hospitalization. He, unfortunately, passed away from viral sepsis, coagulopathy, and multiple organ failure after 25 days of receiving intubation. The patient tested negative for autoantibodies against IFN-α2 and IFN-ω. Whole exome sequencing revealed three variants across type I IFN production pathways, which were predicted to be loss-of-function (pLOF). The three mutations were predicted to be associated with severe viral infections: monoallelic R488X TLR3, monoallelic His684Arg TLR3, and biallelic Val363Met IRF3. Functional analysis confirmed that they affect the type I IFN pathway.

Antiviral innate immune response is achieved through the induction of type I interferons (IFNs) and their stimulated genes. Viral infected cells trigger the activation of Toll-like receptors, primarily TLR3, and cytosolic receptors, including RIG-I and MDA5 [37]. The activated TLR3 stimulates phosphorylation of IRF3, which translocates into the nucleus to bind the virus-responsive element (VRE) in the interferon promoter site resulting in the expression of the type I IFN genes [38–40]. The interaction of type I IFNs with IFNA receptor complex, namely IFNAR1 and IFNAR2, results in the phosphorylation of STAT1 and STAT2 and their combination with the IRF family, IRF9/P48, forming the ISGF3 complex that ultimately activates the expression of different ISGs including IRF3 and IRF7 [38,41]. The proband was presented with inherited deficiencies in TLR3 and IRF3 genes that could have affected his IFN production. No change in IFNβ production levels were detected following stimulation of PBMC's with poly(I:C) (Fig. 3E), while Western blot revealed lower protein expression of TLR3 and downstream ISGs (RIG1 and MX1) in poly(I:C) stimulated PBMCs (Fig. 3D).

These defects predisposed him to several progressive viral infections, including acute hepatitis B, critical fatal COVID-19, and CMV infection. Zhang et al. have studied the association between variants at 13 loci altering the IFN-I immunity and the severity of COVID-19 by comparing 659 patients with life-threatening pneumonia and 534 patients with mild or no symptoms [10]. In their study, 23 patients presented with 24 deleterious loss-of-expression or hypomorphic variants of eight genes, including TLR3, IRF3 [10]. Further, Zhang et al. study revealed that in COVID-19, TLR3, and IRF3 variants conferred autosomal dominant (AD) modes of inheritance [10]. The proband had two monoallelic TLR3 variants and one biallelic IRF3 variant, which follows the above mentioned COVID-19 model of inheritance. Interestingly, in the above cohort, one patient was found to have two deleterious variants, while in our patient, three variants were linked to his progressive SARS-CoV-2 infection. We have plotted the protein position of the proband relative to that reported by Zhang et al. for the above mentioned two genes in Fig. 2A and E. The effect of TLR3 variants on the susceptibility to viral infections, including HBV [42], Herpes Simplex Virus (HSV-1) [43,44], Influenza A virus (IAV) [7], and SARS-CoV-2 [10] have been reported in several human association studies.

The proband had a heterozygous Arg488* TLR3 variant, which caused a stop codon in the middle of the protein's leucine-rich repeats (LRRs) of the ectodomain. This variant was predicted to have a functional impact as it was a highly conserved exposed residue, as shown in Fig. 2C. Additionally, the patient had a missense heterozygous TLR3 variant, His684Arg. The results of the luciferase assay showed that the IFN-β1 promoter activity was reduced by approximately 31% and 42% due to the Arg488* and His684Arg TLR3

mutations, respectively (Fig. 4A). The TA cloning results revealed that the TLR3 variants were on the same allele (Fig. 4C). The observation that the stopgain Arg488* mutation is located upstream of the missense variant His684Arg suggests that the latter is unlikely to be the primary cause of the patient's defect. It is more probable that the stopgain Arg488* TLR3 variant is responsible for the patient's vulnerability to acute HBV, critical progressive COVID-19 disease, and may have also contributed to their CMV infectivity. The proband TLR3 variant's protein position (Arg488*) is close to Pro554Ser and Pro680Leu previously reported in (IAV) [7] and Ser339fs and Pro554Ser variants that were associated with critical COVID-19 [10] (Fig. 2A).

The biallelic IRF3 Val363Met variant positioned in the central regulatory domain (RD) and confirmed by luciferase assay to result in a two-third reduction of IFN-β1 promoter activity, could have contributed to his defective TLR3-IRF3 signaling, as observed with negative IFN induction in patient's PBMCs following the poly(I:C) stimulation. Glu49del and Asn146Lys variants, localized in the N-terminal DNA-binding domain (DBD), were previously associated with severe COVID-19 [10] (Fig. 2E). Another variant (Arg285Gln) presented as heterozygous loss-of-function and localized in RD was associated with impaired IFN responses to HSV-1 infection by affecting IRF3 phosphorylation at S386 and subsequently its activation of transcription [45]. We have found the Val363Met variant to significantly reduce IFN-β1 promoter activity by two-thirds and, therefore, could have also affected the transcription function of IRF3 (Fig. 4B).

This is a complex case of IEIs predisposing to severe viral infections. On admission, the patient reported a history of recurrent infection but did not have any chronic disease and was on no treatment. He was admitted with unremarkable respiratory involvement but had elevated markers of sepsis as well as liver and renal organ failure. He had acute HBV infection and was tested positive for CMV and SARS-CoV-2. The genetic testing revealed deficiencies in multiple immune genes, of which TLR3 and IRF3 could be attributed to his susceptibility to viral infections. Considering hepatitis B infection is not known to be a risk factor for severe COVID-19 disease [46, 47], the critical progressive fatal course of his COVID-19 could only be justified by his underlying IEIs. The limitations inherent in our study must be acknowledged. Our assessment of the impact of these multiple genetic mutations relied on an in-vitro model, and further validation through in-vivo animal models is imperative to confirm the clinical significance and relevance of these genetic variations in a more dynamic and complex biological context.

Ethics statement

This study was approved by Dubai Scientific Research Ethics Committee (DSREC). Written, informed consent was obtained from all study participants prior to inclusion.

Data availability statement

The data will be made available on reasonable request.

CRediT authorship contribution statement

Narjes Saheb Sharif-Askari: Writing – review & editing, Writing – original draft, Visualization, Validation, Software, Methodology, Investigation, Formal analysis, Data curation, Conceptualization. **Shirin Hafezi:** Writing – review & editing, Writing – original draft, Investigation, Data curation, Conceptualization. **Fatemeh Saheb Sharif-Askari:** Writing – review & editing, Writing – original draft, Validation, Formal analysis, Data curation, Conceptualization. **Hawra Ali Hussain Alsayed:** Writing – review & editing, Writing – original draft, Software, Investigation, Data curation, Conceptualization. **Samrein B. M. Ahmed:** Writing – review & editing, Writing – original draft, Methodology, Investigation, Conceptualization. **Habiba S. Alsafar:** Writing – review & editing, Writing – original draft, Formal analysis, Conceptualization. **Rabih Halwani:** Writing – review & editing, Writing – original draft, Validation, Supervision, Resources, Conceptualization.

Declaration of competing interest

The authors declare that they have no known competing financial interests or personal relationships that could have appeared to influence the work reported in this paper.

Acknowledgments

This research has been financially supported by Al Jalila Foundation Seed Grant (AJF202019).

Appendix A. Supplementary data

Supplementary data to this article can be found online at https://doi.org/10.1016/j.heliyon.2024.e29338.

References

[1] H. Chen, J. Guo, C. Wang, F. Luo, X. Yu, W. Zhang, et al., Clinical characteristics and intrauterine vertical transmission potential of COVID-19 infection in nine pregnant women: a retrospective review of medical records, Lancet 395 (10226) (2020) 809–815.
[2] C. Huang, Y. Wang, X. Li, L. Ren, J. Zhao, Y. Hu, et al., Clinical features of patients infected with 2019 novel coronavirus in Wuhan, China, Lancet 395 (10223) (2020) 497–506.
[3] C. Rothe, M. Schunk, P. Sothmann, G. Bretzel, G. Froeschl, C. Wallrauch, et al., Transmission of 2019-nCoV infection from an asymptomatic contact in Germany, N. Engl. J. Med. 382 (10) (2020) 970–971.
[4] M.L. Holshue, C. DeBolt, S. Lindquist, K.H. Lofy, J. Wiesman, H. Bruce, et al., First case of 2019 novel coronavirus in the United States, N. Engl. J. Med. 382 (10) (2020) 929–936.
[5] M.J. Ciancanelli, S.X. Huang, P. Luthra, H. Garner, Y. Itan, S. Volpi, et al., Infectious disease. Life-threatening influenza and impaired interferon amplification in human IRF7 deficiency, Science 348 (6233) (2015) 448–453.
[6] N. Hernandez, I. Melki, H. Jing, T. Habib, S.S.Y. Huang, J. Danielson, et al., Life-threatening influenza pneumonitis in a child with inherited IRF9 deficiency, J. Exp. Med. 215 (10) (2018) 2567–2585.
[7] H.K. Lim, S.X.L. Huang, J. Chen, G. Kerner, O. Gilliaux, P. Bastard, et al., Severe influenza pneumonitis in children with inherited TLR3 deficiency, J. Exp. Med. 216 (9) (2019) 2038–2056.
[8] E. Jouanguy, V. Beziat, T.H. Mogensen, J.L. Casanova, S.G. Tangye, S.Y. Zhang, Human inborn errors of immunity to herpes viruses, Curr. Opin. Immunol. 62 (2020) 106–122.
[9] Zhang S.Y., Herpes simplex virus encephalitis of childhood: inborn errors of central nervous system cell-intrinsic immunity, Hum. Genet. 139 (6-7)(2020) 911-918.
[10] Q. Zhang, P. Bastard, Z. Liu, J. Le Pen, M. Moncada-Velez, J. Chen, et al., Inborn errors of type I IFN immunity in patients with life-threatening COVID-19, Science 370 (6515) (2020).
[11] T. Asano, B. Boisson, F. Onodi, D. Matuozzo, M. Moncada-Velez, M.R.L. Maglorius Renkilaraj, et al., X-linked recessive TLR7 deficiency in ~1% of men under 60 years old with life-threatening COVID-19, Sci Immunol. 6 (62) (2021).
[12] D. Matuozzo, E. Talouarn, A. Marchal, P. Zhang, J. Manry, Y. Seeleuthner, et al., Rare predicted loss-of-function variants of type I IFN immunity genes are associated with life-threatening COVID-19, Genome Med. 15 (1) (2023) 22.
[13] Genomewide Association Study of Severe Covid-19 with Respiratory Failure, N. Engl. J. Med. 383 (16) (2020) 1522–1534.
[14] T.H. Karlsen, Understanding COVID-19 through genome-wide association studies, Nat. Genet. 54 (4) (2022) 368–369.
[15] M. Mousa, H. Vurivi, H. Kannout, M. Uddin, N. Alkaabi, B. Mahboub, et al., Genome-wide association study of hospitalized COVID-19 patients in the United Arab Emirates, EBioMedicine 74 (2021).
[16] H. Abolhassani, A. Vosughimotlagh, T. Asano, N. Landegren, B. Boisson, S. Delavari, et al., X-linked TLR7 deficiency underlies critical COVID-19 pneumonia in a male patient with ataxia-telangiectasia, J. Clin. Immunol. 42 (1) (2022) 1–9.
[17] R. Ameratunga, S.-T. Woon, V.L. Bryant, R. Steele, C. Slade, E.Y. Leung, et al., Clinical implications of digenic inheritance and epistasis in primary immunodeficiency disorders, Front. Immunol. 8 (2018).
[18] M.J. Massaad, J. Zhou, D. Tsuchimoto, J. Chou, H. Jabara, E. Janssen, et al., Deficiency of base excision repair enzyme NEIL3 drives increased predisposition to autoimmunity, J. Clin. Investig. 126 (11) (2016) 4219–4236.
[19] R. Hoyos-Bachiloglu, J. Chou, C.N. Sodroski, A. Beano, W. Bainter, M. Angelova, et al., A digenic human immunodeficiency characterized by IFNAR1 and IFNGR2 mutations, J. Clin. Investig. 127 (12) (2017) 4415–4420.
[20] NIH. COVID-19 Treatment Guidelines Panel. Coronavirus Disease 2019 (COVID-19) Treatment Guidelines. National Institutes of Health.Available at: https://www.covid19treatmentguidelines.nih.gov/. Access date: 9/9/20021..
[21] A. Alamer, A.A. Alrashed, M. Alfaifi, B. Alosaimi, F. AlHassar, M. Almutairi, et al., Effectiveness and safety of favipiravir compared to supportive care in moderately to critically ill COVID-19 patients: a retrospective study with propensity score matching sensitivity analysis, Curr. Med. Res. Opin. 37 (7) (2021) 1085–1097.
[22] Q. Ma, J. Liu, Q. Liu, L. Kang, R. Liu, W. Jing, et al., Global percentage of asymptomatic SARS-CoV-2 infections among the tested population and individuals with confirmed COVID-19 diagnosis: a systematic review and meta-analysis, JAMA Netw. Open 4 (12) (2021) e2137257.
[23] S. Al-Muhsen, N.S. Al-Numair, N. Saheb Sharif-Askari, R. Basamh, B. Alyounes, A. Jabaan, et al., Favipiravir effectiveness and safety in hospitalized moderate-severe COVID-19 patients: observational prospective multicenter investigation in Saudi Arabia, Front. Med. 9 (2022) 826247.
[24] www.cdc.gov.Available from:: https://www.cdc.gov/coronavirus/2019-ncov/lab/guidelines-clinical-specimens.html. Access date: 9/September/2020 [.
[25] H. Li, R. Durbin, Fast and accurate short read alignment with Burrows–Wheeler transform, Bioinformatics 25 (14) (2009) 1754–1760.
[26] M.A. DePristo, E. Banks, R. Poplin, K.V. Garimella, J.R. Maguire, C. Hartl, et al., A framework for variation discovery and genotyping using next-generation DNA sequencing data, Nat. Genet. 43 (5) (2011) 491–498.
[27] J.-L. Casanova, L. Abel, Mechanisms of viral inflammation and disease in humans, Science 374 (6571) (2021) 1080–1086.
[28] T. Asano, B. Boisson, F. Onodi, D. Matuozzo, M. Moncada-Velez, M.R.L. Maglorius Renkilaraj, et al., X-linked recessive TLR7 deficiency in ~1% of men under 60 years old with life-threatening COVID-19, Science Immunology 6 (62) (2021) eabl4348.
[29] J. Choe, M.S. Kelker, I.A. Wilson, Crystal structure of human Toll-like receptor 3 (TLR3) ectodomain, Science. 309 (5734) (2005) 581–585.
[30] B. Zhao, C. Shu, X. Gao, B. Sankaran, F. Du, C.L. Shelton, et al., Structural basis for concerted recruitment and activation of IRF-3 by innate immune adaptor proteins, Proc Natl Acad Sci U S A. 113 (24) (2016) E3403–E3412.
[31] H. Ashkenazy, S. Abadi, E. Martz, O. Chay, I. Mayrose, T. Pupko, et al., ConSurf 2016: an improved methodology to estimate and visualize evolutionary conservation in macromolecules, Nucleic Acids Res. 44 (W1) (2016) W344–W350.
[32] J.S. Muhammad, N. Saheb Sharif-Askari, Z.-G. Cui, M. Hamad, R. Halwani, SARS-CoV-2 infection-induced promoter hypomethylation as an epigenetic modulator of heat shock protein A1L (HSPA1L) gene, Front. Genet. 12 (129) (2021).
[33] S. Goel, F. Saheb Sharif-Askari, N. Saheb Sharif-Askari, B. Mdkhana, B. Mahboub, A.M. Zakri, et al., SARS-CoV-2 Switches 'on' MAPK and NFF06B B signaling via the reduction of nuclear DUSP1 and DUSP5 expression, Front. Pharmacol. 12 (2021) 404.
[34] S.V. Kuchipudi, M. Tellabati, R.K. Nelli, G.A. White, B.B. Perez, S. Sebastian, et al., 18S rRNA is a reliable normalisation gene for real time PCR based on influenza virus infected cells, Virol. J. 9 (1) (2012) 1–7.
[35] P. Bastard, A. Gervais, T. Le Voyer, J. Rosain, Q. Philippot, J. Manry, et al., Autoantibodies neutralizing type I IFNs are present in ~4% of uninfected individuals over 70 years old and account for ~20% of COVID-19 deaths, Sci Immunol 6 (62) (2021).
[36] J. Zhu, K. Smith, P.N. Hsieh, Y.K. Mburu, S. Chattopadhyay, G.C. Sen, et al., High-throughput screening for TLR3-IFN regulatory factor 3 signaling pathway modulators identifies several antipsychotic drugs as TLR inhibitors, J. Immunol. 184 (10) (2010) 5768–5776.
[37] K. Honda, A. Takaoka, T. Taniguchi, Type I inteferon gene induction by the interferon regulatory factor family of transcription factors, Immunity 25 (3) (2006) 349–360.
[38] P.M. Pitha, M.S. Kunzi, Type I interferon: the ever unfolding story, in: P.M. Pitha (Ed.), Interferon: the 50th Anniversary, Springer Berlin Heidelberg, Berlin, Heidelberg, 2007, pp. 41–70.
[39] U. Weidle, C. Weissmann, The 5'-flanking region of a human IFN-alpha gene mediates viral induction of transcription, Nature 303 (5916) (1983) 442–446.
[40] D. Thanos, T. Maniatis, Virus induction of human IFNβ gene expression requires the assembly of an enhanceosome, Cell 83 (7) (1995) 1091–1100.
[41] J.E. Darnell Jr., I.M. Kerr, G.R. Stark, Jak-STAT pathways and transcriptional activation in response to IFNs and other extracellular signaling proteins, Science 264 (5164) (1994) 1415–1421.
[42] A. Al-Qahtani, M. Al-Ahdal, A. Abdo, F. Sanai, M. Al-Anazi, N. Khalaf, et al., Toll-like receptor 3 polymorphism and its association with hepatitis B virus infection in Saudi Arabian patients, J. Med. Virol. 84 (9) (2012) 1353–1359.

[43] S.Y. Zhang, E. Jouanguy, S. Ugolini, A. Smahi, G. Elain, P. Romero, et al., TLR3 deficiency in patients with herpes simplex encephalitis, Science 317 (5844) (2007) 1522–1527.
[44] Y. Guo, M. Audry, M. Ciancanelli, L. Alsina, J. Azevedo, M. Herman, et al., Herpes simplex virus encephalitis in a patient with complete TLR3 deficiency: TLR3 is otherwise redundant in protective immunity, J. Exp. Med. 208 (10) (2011) 2083–2098.
[45] L.L. Andersen, N. Mørk, L.S. Reinert, E. Kofod-Olsen, R. Narita, S.E. Jørgensen, et al., Functional IRF3 deficiency in a patient with herpes simplex encephalitis, J. Exp. Med. 212 (9) (2015) 1371–1379.
[46] J.W. Choe, Y.K. Jung, H.J. Yim, G.H. Seo, Clinical effect of hepatitis B virus on COVID-19 infected patients: a nationwide population-based study using the Health insurance review & assessment service database, J Korean Med Sci. 37 (4) (2022).
[47] S.H. Kang, D.H. Cho, J. Choi, S.K. Baik, J.G. Gwon, M.Y. Kim, Association between chronic hepatitis B infection and COVID-19 outcomes: a Korean nationwide cohort study, PLoS One 16 (10) (2021) e0258229.